HHS Public Access

Author manuscript

Appl Magn Reson. Author manuscript; available in PMC 2020 March 01.

Published in final edited form as:

Appl Magn Reson. 2019 March ; 50(1-3): 333–345. doi:10.1007/s00723-018-1078-y.

250 MHz Rapid Scan Cross Loop Resonator

Laura A. Buchanan[1], **Lukas B. Woodcock**[1], **George A. Rinard**[2], **Richard W. Quine**[2], **Yilin Shi**[1], **Sandra S. Eaton**[1], and **Gareth R. Eaton**[1]

[1]Department of Chemistry and Biochemistry, University of Denver, Denver, CO 80210

[2]School of Engineering and Computer Science, University of Denver, Denver, CO 80210

Abstract

A 25 mm diameter 250 MHz crossed-loop resonator was designed for rapid scan electron paramagnetic resonance imaging. It has a saddle coil for the driven resonator and a fine wire, loop gap resonator for the sample resonator. There is good separation of E and B fields and high isolation between the two resonators, permitting a wide range of sample types to be measured. Applications to imaging of nitroxide, trityl, and LiPc samples illustrate the utility of the resonator. Using this resonator and a trityl sample the signal-to-noise of a rapid scan absorption spectrum is about 20 times higher than for a first-derivative CW spectrum.

Introduction

A wide variety of resonators has been used for in vivo electron paramagnetic resonance (EPR) imaging and other low-frequency EPR spectroscopy and relaxation measurements. Early low-frequency spectrometers have been comprehensively reviewed [1]. Resonator experience in the Denver and Chicago labs at 250 MHz was summarized in Ref. [2], and a recent paper implemented in vivo rapid scan imaging of nitroxide radicals using a cross loop resonator (CLR) [3]. Examples of resonators that have been used for imaging and physiology studies in other labs at frequencies below 500 MHz include a 221 MHz saddle coil with 13.5 mm diameter and 23.5 mm long [4]; a 300 MHz parallel coil resonator with ca. 25 mm diameter, 50 mm long [5, 6] or 25 mm long [7]; and a 55 mm diameter loop at 300 MHz [8].

The CLR concept [9], first implemented at S-band, has been extended from 250 MHz [10] to X-band [11]. Originally designed for pulsed EPR, the CLR concept has also been implemented for rapid scan EPR [12] by using thin wire construction to minimize eddy currents by breaking up the induced magnetic field on the conducting surfaces of the resonator [13]. The two resonators of the CLR are commonly called the driven resonator and the sample resonator. A current challenge is to create a resonator with room for a mouse, physiologic support apparatus and specialized experimental devices, such as perfusion pumps, while maintaining good signal-to-noise, ease of tuning, and high isolation between the two resonators of the CLR. Progress toward this ideal is presented in this paper. We

Corresponding Author Professor Gareth R. Eaton, Department of Chemistry and Biochemistry, University of Denver, Denver, CO 80210, 303-871-2980, geaton@du.edu.

report a CLR with 25 mm internal diameter to accommodate a mouse, a sample resonator whose frequency can be adjusted to be the same as that of the driven resonator for samples with varying dielectric loss, and isolation of up to 60 dB between the two resonators. Two-dimensional spectral-spatial imaging of several phantoms are presented to illustrate imaging performance. We built 2 of these resonators, confirming reproducibility of the construction. Most of the tests were performed on one resonator, which was then sent to University of Chicago where the mouse measurements were made. The CW and rapid scan signal-to-noise comparisons were made on the other resonator, using a trityl sample.

Resonator design and test results

The design of the 250 MHz resonator, as shown in Figures 1 and 2, is for in vivo measurements, with the mouse in a horizontal position. For rapid scan imaging it is important to minimize eddy currents in the materials of the resonator. All dielectric parts of the CLR except the resonator tubes were 3-D printed with polylactic acid (PLA); the resonator tubes were 3-D printed with high impact polystyrene (HIPS). The equivalent circuits for the two resonators are shown in Figure 3. All fixed capacitors are Voltronics, series 5, non-magnetic chip capacitors. The variable capacitor indicated in Figure 3 is a Johanson, JMC #5761. The microwave excitation is incident upon the driven resonator, which has a larger diameter than the sample resonator. The driven resonator is a saddle coil resonator constructed of 0.25 in. (6.4 mm) wide adhesive backed copper foil. It is 25 mm average length and is mounted on the outside of a tube, 36 mm OD, 33 mm ID and 38 mm long. The EPR signal is induced in the smaller (higher filling factor ~80%) sample resonator and directed to the signal detection system. The sample resonator is a loop gap resonator (LGR) constructed of 40 parallel turns of No. 38, 0.004 in. (0.1 mm) diameter bare copper wire. It is 25 mm long and is mounted on a tube, 27.9 mm OD, 26 mm ID, and 66.6 mm long, which is the length of the RF shield. This wire resonator is similar to a solid metal one, except that the wire construction allows the RF magnetic field from the driven resonator to easily penetrate it. The plastic RF shield is 73 mm OD, 70.5 mm ID and 60.5 mm long. It is painted on the inside with silver paint. The coax cables that connect the source to the driven resonator and the output from the sample resonator to the detection system contain bazooka baluns to match the properties of the resonator to the transmission lines. The baluns were constructed by replacing the center conductor of a 24.9 cm length of Haverhill HC90009–1, 0.141 in. coaxial cable with a length of Haverhill HC10009–1, 0.047 in, coaxial cable. The outer conductors of both cables are connected together at the input.

The CLR is similar, in design, to a 19 mm i.d. CLR designed for pulse imaging [2, 14], which used four loops of copper foil for the sample resonator and an Alderman-Grant design for the driven resonator.

A balun is a bal<u>anced to un</u>balanced network. Some two-terminal devices are balanced to ground, which means that the impedance to ground is the same for each terminal; the resonators in this CLR are like this. As shown in Figure 3, there are two equal, coupling capacitors in the resonators to try to maintain this balance. The coaxial cable used to connect the transmission lines to the resonators is unbalanced; one of the terminals <u>is</u> ground, or as close as possible. If the coax is connected directly to the balanced resonator, it upsets the

balance to ground of the resonator and undesirable currents will flow on the outside of the coax and inside of the RF shield. This may not have much effect on the resonant frequency, but it can affect the isolation, because the unbalance causes undesirable fields that can link the two resonators. In some unbalanced cases, adjusting the resonators so that they are not physically perpendicular, may improve isolation by causing a coupling that helps cancel the unbalanced pick-up. However, since amplitude, phase and physical orientation are involved, we cannot expect this to be very useful. A more straightforward approach is to reduce the unbalance in the circuit.

A bazooka balun achieves its operation by means of a quarter wave coaxial, transmission line shield around the feed coax. Since it is shorted at the feed end, it is an open at the resonator end. This reduces the tendency for current to flow on the outside of the coax. Unfortunately, a bazooka balun, because it uses a quarter wave coaxial type resonant structure, is very narrow band. Therefore, optimally the balun is tuned to the resonant frequency of the resonator. However, a challenge arises due to the change of the resonant frequency with different samples, which may shift the frequency outside the effective bandwidth of the balun.

The frequency of the sample resonator may vary due to the dielectric properties of the sample. In this resonator the frequency is adjustable to match the frequency of the driven resonator, using the knurled knob below the animal. The tuning adjusts a nonmagnetic variable capacitor. In other resonators built in our lab a tuning tool is inserted into the adjustment mechanism of the driven resonator to adjust the frequency. The added capacitance of the tuning tool and the operator change the frequency independent of the intended capacitance change, which makes adjustment tedious. In the present design this problem is avoided by using spring-loaded tuning shaft that is left in place throughout the measurements.

To tune this CLR, the first step is to adjust the source frequency to the frequency of the driven resonator. The frequency of the sample resonator is then adjusted using the knurled knob at the base of the 25 mm resonator. The two resonators are designed to be electrically orthogonal. Small manufacturing non-orthogonalities and the effect of asymmetric loading by the sample can be significant and can be corrected for by small physical rotation of one of the resonators about the pivot point identified in Figure 2. For ease of adjustment while a mouse is in the resonator, the isolation tuning adjustment is available to the operator as a knob above the sample.

Characterization of the driven and sample resonators and the isolation between them are summarized in Table 1. The table includes data for a CLR containing a live mouse, which was measured in H. J. Halpern’s lab in the Department of Radiation and Cellular Oncology, University of Chicago. The measurements at the University of Denver were made using a network analyzer (HP8719D) with the sample resonator empty and with a sample of water filling the resonator. The water sample was a glass cylinder 25 mm OD, 25 mm long, with flat top and bottom and a 6 mm OD filling tube. The driven resonator is a fixed-frequency resonator and is largely unaffected by lossy aqueous samples. The efficiencies were calculated by comparing the incident power required to achieve the same degree of

saturation for a coal sample measured at 254 MHz in the new resonators and at 9.5 GHz in a Bruker SHQ resonator for which the known efficiency is 2 G/$\sqrt{W}$. The efficiency of the driven resonator is about 0.14 G/$\sqrt{W}$ and the efficiency of the sample resonator is about 0.25 G/$\sqrt{W}$. For comparison with prior low-frequency resonators for pulsed EPR imaging, the Alderman-Grant resonator described in Ref.[2] and [14] with 23 mm i.d. is the closest to our resonator. It has $\Lambda = 0.12G/\sqrt{W}$ at Q = 11. Our rapid scan resonator has $\Lambda = 0.25$ G/√W at Q = 78. The pulse data reported for the parallel wire type resonator used for low-frequency EPR imaging [5] shows that their 25 mm i.d. resonator had an efficiency of about 0.14 G/√W with Q = 20. Thus, the several designs exhibit the expected tradeoffs of size and Q.

The separation of E and B fields was so good that introducing a lossy, high dielectric, water sample in a glass container that filled the resonator reduced the frequency of the driven resonator by 0.4 MHz relative to the empty resonator. When a live mouse was in the resonator, the frequency decreased by less than a MHz (Table 1). These frequency changes are well within the tuning range of the sample resonator. The sample resonator could also be used with a small sample with negligible effect on the tuning, demonstrating the wide range of samples that can be imaged in this resonator. The isolation between the two resonators is stable up to about 0.5 W of continuous RF power.

Magnetic field scan coils

The rapid magnetic field scan coils (square coils shown in Figure 1) were constructed of 100 turns of 250/46 Litz wire. The pair of coils has 86 mm average width and 46 mm average spacing. The cross-section of the windings measured 10.2 by 10.2 mm. The experimentally determined coil constant was 18.8 G/A. The coil constant was determined by measuring the spacings of trityl-CD_3 ^{13}C hyperfine after deconvolution to obtain the slow scan spectrum and comparing those with literature values [15]. The inductance was measured by resonating the rapid scan coil circuit with known capacitor values. The resonant frequency (f) and capacitor value (C) were used to solve for the inductance (L) using eq. 1. The calculated inductance of the coils is 3.5 mH.

$$L = \frac{1}{(2\pi f)^2 C} \quad (1)$$

The scan coils were driven with the rapid scan coil driver (RSCD) described in Ref. [16]. Scan frequencies were chirped from about 1.2 kHz to 7.5 kHz using a ramped sinusoidal wave generated by the RSCD. The complex detected signal from the empty resonator was digitized over the time interval of the chirp. The absolute value (magnitude) of the Fourier transform of the time response is plotted in Figure 4 and designated as the mechanical resonance background. It was recorded for three conditions: $B_0 = 0$ with no gradient, $B_0 =$ 90 G with no gradient, and B_0 90 G with gradient. This background is attributed to motor effects due to the rapid scan field interacting with main magnetic field. The background amplitude is relatively small when no main magnetic field or z-gradient field is applied. Application of a z gradient field increased the background amplitude at scan frequencies below 1.8 kHz and around 2.5 kHz.

Samples

Two lithium phthalocyanine (LiPc) samples (1.1 mm ID x 3 mm long) were flame sealed after being evacuated on a high vacuum line. A 0.1 mM tris 8-carboxyl-2,2,6,6 tetra[2-(1-hydroxyethyl)]-benzo(1,2-d:4,5-d) bis(1,3) dithiol-4-ylmethyl radical sodium salt (OX63) solution was prepared in 2 mM HEPES (4-(2-hydroxyethyl)-1-piperazine-ethanesulfonic acid) buffer. Aqueous solutions of 1 mM 4-hydroxy-2,2,6,6-tetramethylpiperidin-1-oxyl (Tempol, SigmaAldrich, St. Louis, MO), and ^{15}N per-deuterated Tempone (PDT, Cambridge Isotope Laboratories, Tewksbury, MA) solutions also were prepared. Aqueous solutions were bubbled with N_2 before flame sealing.

Continuous wave and rapid scan comparison

The second, duplicate, 250 MHz CLR was used to obtain continuous wave (CW) and rapid scan spectra of a 0.1 mM degassed OX63 sample (25 mm OD diameter x 16 mm OD long that) were recorded using the 250 MHz spectrometer [16] previously described. The signal to noise of the CW and rapid scan spectra were calculated as the maximum minus minimum signal amplitude divided by the standard deviation of noise corresponding to the first 75 points in the spectra. The frequency of the resonator with the OX63 sample present was 260.69 MHz. Sinusoidal rapid scans were generated with a resonated coil driver [15] at 30 kG/s. Incident powers for collection of CW and rapid scan spectra were selected by inspecting power saturation curves and selecting the maximum power for which the amplitude of the EPR signal was within 95% of that predicted by linear extrapolation from low power. CW parameters were as follows: B_0 = 93.53 G, modulation frequency = 10 kHz, modulation amplitude = 24 mG, modulation phase = 45°, incident power = 0.4 mW, conversion time = 5.2 ms, scan time = 5.32 s, sweep width = 3 G, 1024 points, 1-point smooth. Rapid scan parameters were as follows: B_0 = 93.53 G, scan frequency = 3.2 kHz, sweep width = 3 G, incident power = 5.2 mW, 4096 averages, time base = 20 ns, 65536 points, scan time = 5.37 s. Rapid scan spectra were collected in quadrature and deconvolved using the algorithm described in [17]. Pseudo-modulation of the rapid scan spectra in Bruker Xepr software (version 2.6b.167) using 24 mG was done to obtain the first derivative spectrum which reduced the signal to noise compared to the absorption spectrum. The signal to noise of the rapid scan absorption spectrum, pseudo-modulated rapid scan spectrum, and CW spectrum were 400, 173, and 18, respectively (Figure 5). The improved signal-to-noise for rapid scan is consistent with prior observations for other samples and resonators [18]. X-band rapid scan of nitroxides and other broad-line species were reported in many prior studies, both at low microwave frequencies [3, 12, 19] and at X-band with small reflection resonators [20, 21].

Application to EPR imaging

Rapid scan EPR imaging was achieved using the 250 MHz spectrometer [22] and resonated coil driver [16] previously described. Magnetic field gradients up to 10 G/cm in the z-direction were created with the coils described in Ref. [23]. The main improvements in the spectrometer since the description in 2002 include replacing the power supplies with Ethernet controlled power supplies manufactured by CAEN (FAST-PS-1k5 30–50) for main

field and (FAST-PS 2040–600) for the z gradient and controlling the field and z-gradient with code written in Python within the Bruker Xepr software system. A version of Xepr that includes an Xepr API is required to run locally written python programs. 2-D spectral-spatial images were reconstructed using the algorithm developed in Ref. [24].

2D Images

One phantom consisted of two LiPc samples separated by 1 cm along the z-axis (Figure 6). A 2-D spectral spatial image collected along the z axis is shown in Figure 7. The z gradient was varied between ± 5 G/cm in 0.05 G/cm steps. A rapid scan frequency of 2.213 kHz with 30 G sweep width was used to acquire the spectra. The power was adjusted so that the LiPc signal amplitude was in the linear response range. The full width half maximum (FWHM) absorption line width of the zero gradient spectrum was 200 mG. Spectral slices for the approximate centers of the two samples (z = −0.27 and +0.81 cm) had a measured line width of 240 mG FWHM.

To obtain the image shown in Figure 7 the resonator and sample were positioned at the vertical position that corresponds to the central axis of the main magnetic field. If the phantom is vertically offset from the center by about 2 cm, the off-axis fields generated by the gradient coils [23, 25] add a contribution to B_0 that increases approximately quadratically with the current in the gradient coils. Figure 8 illustrates the effect of concomitant magnetic field gradients on an image of the two small LiPc samples. The high spectral and spatial resolution of this sample facilitated observation of these effect of the concomitant gradients, which are a well-known phenomenon in low-field MRI [26–29]. The distortions in the image in Figure 8B follow the patterns illustrated in Ref. [26, 28]. Application of a correction to the effective center field for each projection that depended quadratically on the magnitude of the applied gradient (Figure 8C) offsets the effects of the concomitant gradients. The expression for the correction was $\Delta B_0 = 2\times10^{-2}$ (gradient)^2. The resulting corrected image shown in Figure 8D is in good agreement with the image (Figure 7) for the phantom that was properly centered in the vertical dimension.

Another 2-D spectral-spatial image was collected along the z-axis of the aqueous phantom shown in Figure 9. The gradient was varied between ± 10 G/cm in 0.1 G/cm steps for a total of 201 projections. A sinusoidal rapid scan frequency of 2.213 kHz with 75 G sweep width (scan rate of 0.52 MG/s) was used to acquire the spectra. The power was adjusted so that the amplitude of the OX63 signal was in the linear response range. The nitroxides saturate less readily than OX63. The B_1 in the driven resonator was approximately 22 mG. With these parameters the OX63 and nitroxide signals are in the rapid scan regime [30]. The background reduction method described in Ref. [31] was used to acquire the imaging data. The data were acquired in quadrature and the two channels were combined prior to image reconstruction [20, 21]. The resulting image is shown in Figure 10. The line widths of OX63, PDT and Tempol in the zero gradient spectrum were 0.36, 0.55, and 2 G, respectively. The line widths measured along spectral slices at z = −0.72 and +0.64 cm were 0.74, 1 and 2 G, respectively. The line broadening of the narrow lines in the image is more significant for the extended sample than for the LiPc point samples. The increased linewidth

in the image relative to that in the non-gradient spectrum is attributed to the limited number of projections.

Summary

The features of this new resonator design that contribute to its utility are the good separation of E and B fields and the high isolation between the two resonators. The larger diameter sample resonator should allow room for in vivo imaging of mice with specialized experimental devices. Rapid scan images of aqueous and non-aqueous samples were acquired to demonstrate the wide variety of samples that can be imaged with this resonator. For a trityl sample the signal-to-noise ratio for rapid scan is about 20 times higher than for CW. This resonator could also be used for pulsed EPR, which is convenient for measurements such as pulsed oximetry using trityl radicals [32].

Supplementary Material

Refer to Web version on PubMed Central for supplementary material.

Acknowledgments

The spectrometer pulse and rapid scan development was supported in part by NIH NCI AIP grant CA177744, and in part by NIH P41EB002034 (Howard J. Halpern, PI).

References

1. Eaton SS Eaton GR: Biol. Magn. Reson 21, 59–114 (2004).
2. Rinard GA, Quine RW, Buchanan LA, Eaton SS, Eaton GR, Epel B, Sundramoorthy SV, Halpern HJ: Appl. Magn. Reson 48, 1227–1247 (2017). [PubMed: 29391664]
3. Epel B, Sundramoorthy SV, Krzykowska-Serda M, Maggio MC, Tseytlin M, Eaton GR, Eaton SS, Rosen GM, Kao JPY, Halpern HJ: J. Magn. Reson 276, 31–36 (2017). [PubMed: 28092786]
4. Matsumoto S, Yamada K, Hirata H, Yasukawa K, Hyodo F, Ichikawa K, Utsumi H: Magn. Reson. Med 57, 806–811 (2007). [PubMed: 17390363]
5. Devasahayam N, Subramanian S, Murugesan R, Cook JA, Afeworki M, Tschudin R, Mitchell JB, Krishna MC: J. Magn. Reson 142, 168–176 (2000). [PubMed: 10617448]
6. Afeworki M, Gooitzen MD, Devasahayam N, Murugesan R, Cook J, Coffin D, Larsen JA, Mitchell JB, Subramanian S, Krishna MC: Magn. Reson. Med 43, 375–382 (2000). [PubMed: 10725880]
7. Matsumoto K, Chandrika B, Lohman JAB, Mitchell JB, Krishna M, Subramanian S: Magn. Reson. Med 50, 865–874 (2003). [PubMed: 14523974]
8. Hirata H, He G, Deng Y, Salikhov I, Petryakov S, Zweier JL: J. Magn. Reson 190, 124–134 (2008). [PubMed: 18006343]
9. Rinard GA, Quine RW, Ghim BT, Eaton SS, Eaton GR: J. Magn. Reson. A 122, 50–57 (1996).
10. Rinard GA, Quine RW, Eaton GR, Eaton SS: Magn. Reson. Engineer 15, 37–46 (2002).
11. Rinard GA, Quine RW, McPeak J, Buchanan L, Eaton SS, Eaton GR: Appl. Magn. Reson 48, DOI 10.1007/S00723-00017-00945-00722 (2017).
12. Eaton GR Eaton SS, in: Handbook of EPR Spectroscopy: Fundamentals and Methods, Goldfarb D, Stoll S, Ed., 503–520, John Wiley & Sons, 2018.
13. Rinard GA, Quine RW, Biller JR, Eaton GR: Concepts Magn. Reson. B, Magn. Reson. Engineer 37B, 86–91 (2010).
14. Sundramoorthy SV, Epel B, Halpern HJ: J. Magn. Reson 240, 45–51 (2014). [PubMed: 24530507]
15. Trukhan SN, Yudanov VF, Rogozhnikova O, Trukhin D, Bowman MK, Krzyaniak MD, Chen H, Martyanov ON: J. Magn. Reson 233, 29–36 (2013). [PubMed: 23722184]

16. Quine RW, Mitchell DG, Eaton SS, Eaton GR: Conc. Magn. Reson., Magn. Reson. Engineer 41B, 95–110 (2012).
17. Tseitlin M, Rinard GA, Quine RW, Eaton SS, Eaton GR: J. Magn. Reson 208, 279–283 (2011). [PubMed: 21163677]
18. Eaton SS, Quine RW, Tseitlin M, Mitchell DG, Rinard GA, Eaton GR, in: Multifrequency Electron Paramagnetic Resonance: Data and Techniques, Misra SK, Ed., 3–67, Wiley 2014.
19. Eaton SS, Shi Y, Woodcock L, Buchanan LA, McPeak J, Quine RW, Rinard GA, Epel B, Halpern HJ, Eaton GR: J. Magn. Reson 280 140–148 (2017). [PubMed: 28579099]
20. Kittell AW, Camenisch TG, Ratke JJ, Sidabras JW, Hyde JS: J. Magn. Reson 211, 228–233 (2011). [PubMed: 21741868]
21. Yu Z, Liu T, Elajaili H, Rinard GA, Eaton SS, Eaton GR: J. Magn. Reson 258, 58–64 (2015). [PubMed: 26232363]
22. Quine RW, Rinard GA, Eaton SS, Eaton GR: Magn. Reson. Engineer 15, 59–91 (2002).
23. Rinard GA, Quine RW, Eaton SS, Eaton GR, Barth ED, Pelizzari CA, Halpern HJ: Magn. Reson. Engineer 15, 51–58 (2002).
24. Tseitlin M, Biller JR, Elajaili H, Khramtsov V, Dhimitruka I, Eaton GR, Eaton SS: J. Magn. Reson 245, 150–155 (2014). [PubMed: 25058914]
25. Gillies DG, Sutcliffe LH, Symms MR: J.C.S. Faraday Trans 90, 2671–2675 (1994).
26. Volegov PL, Mosher JC, Espy MA, Kraus RHJ: J. Magn. Reson 175, 103–113 (2005). [PubMed: 15869890]
27. Yablonsky DA, Sukstanskii AL, Ackerman JJH: J. Magn. Reson 174, 279–286 (2005). [PubMed: 15862245]
28. Nieminen JO Ilmoniemi RJ: J. Magn. Reson 207, 213–219 (2010). [PubMed: 20884262]
29. Weavers PT, Tao S, Trzasko JD, Frigo LM, Shu Y, Frick MA, Lee S-K, Foo TK-F, Bernstein MA: Magn. Reson. Med 79, 1538–1544 (2010).
30. Mitchell DG, Quine RW, Tseitlin M, Eaton SS, Eaton GR: J. Magn. Reson 214, 221–226 (2012). [PubMed: 22169156]
31. Buchanan LA, Woodcock LB, Quine RW, Rinard GA, Eaton SS, Eaton GR: J. Magn. Reson 293, 1–8 (2018). [PubMed: 29800785]
32. Epel B, Bowman MK, Mailer C, Halpern HJ: Magn. Reson. Med 72, 362–368 (2014). [PubMed: 24006331]

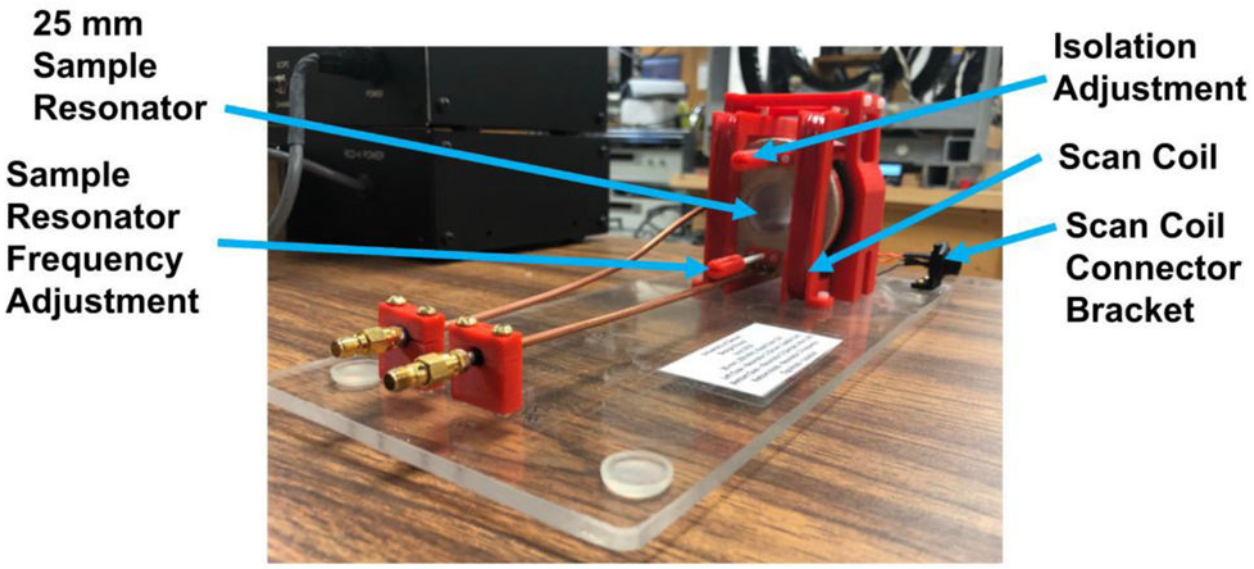

Figure 1.
25 mm, 250 MHz, Rapid Scan, Cross Loop Resonator Assembly. The mechanical structure of the resonator and scan coil assembly was built with a 3D printer using polylactic acid (PLA).

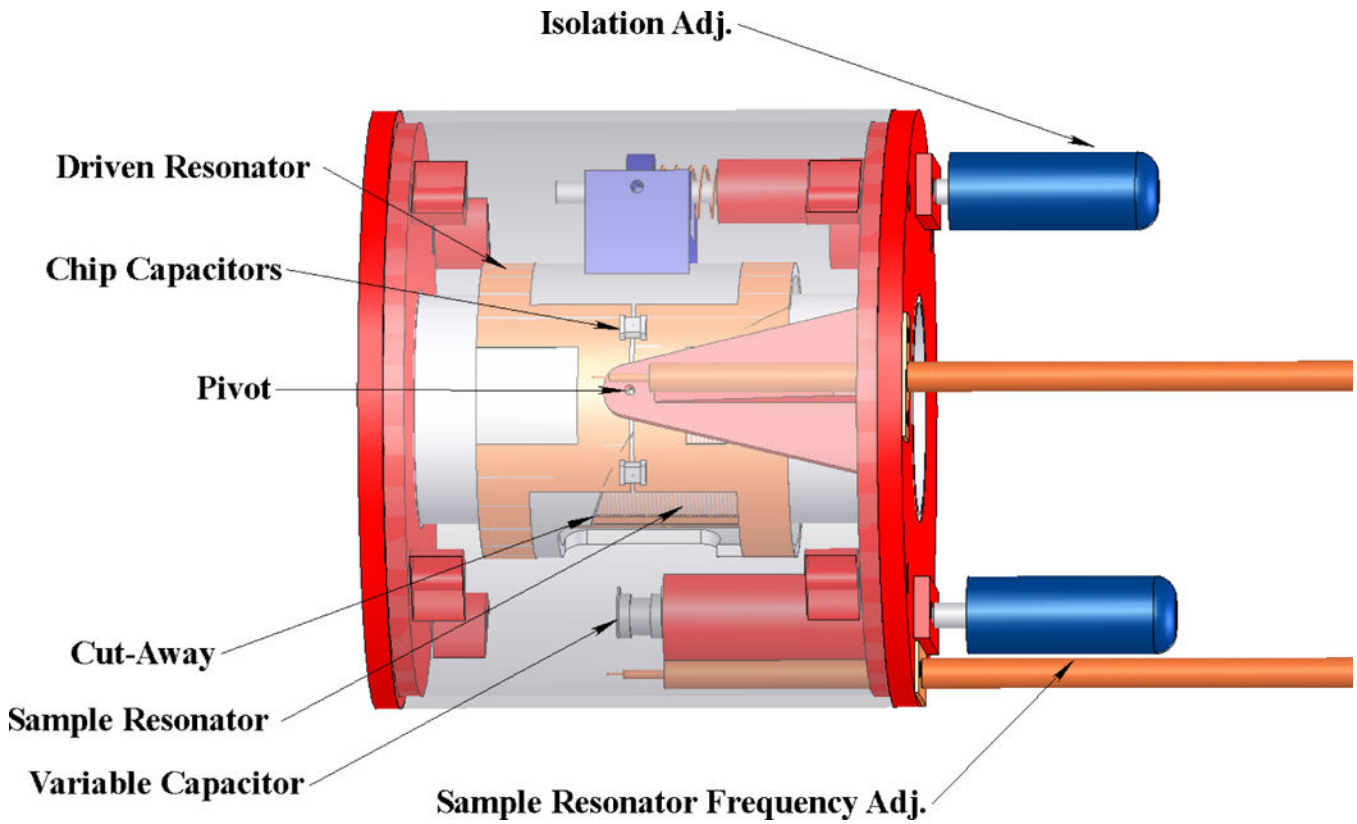

Figure 2.
Internal construction of CLR.

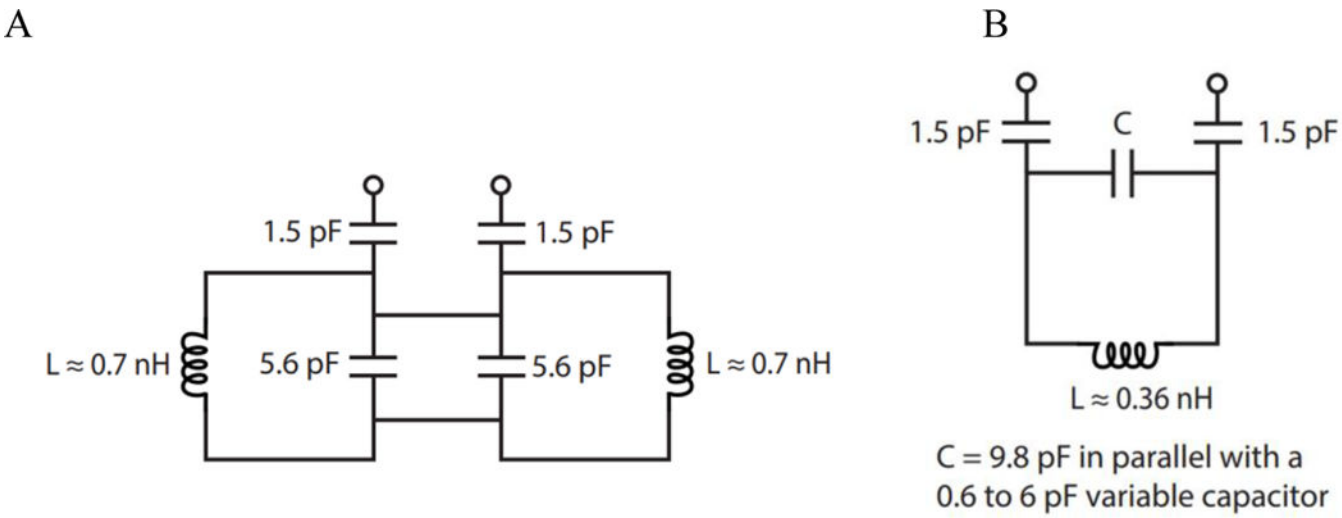

Figure 3.

Equivalent circuit diagrams for (A) Driven resonator, saddle coil and (B) Sample resonator, LGR.

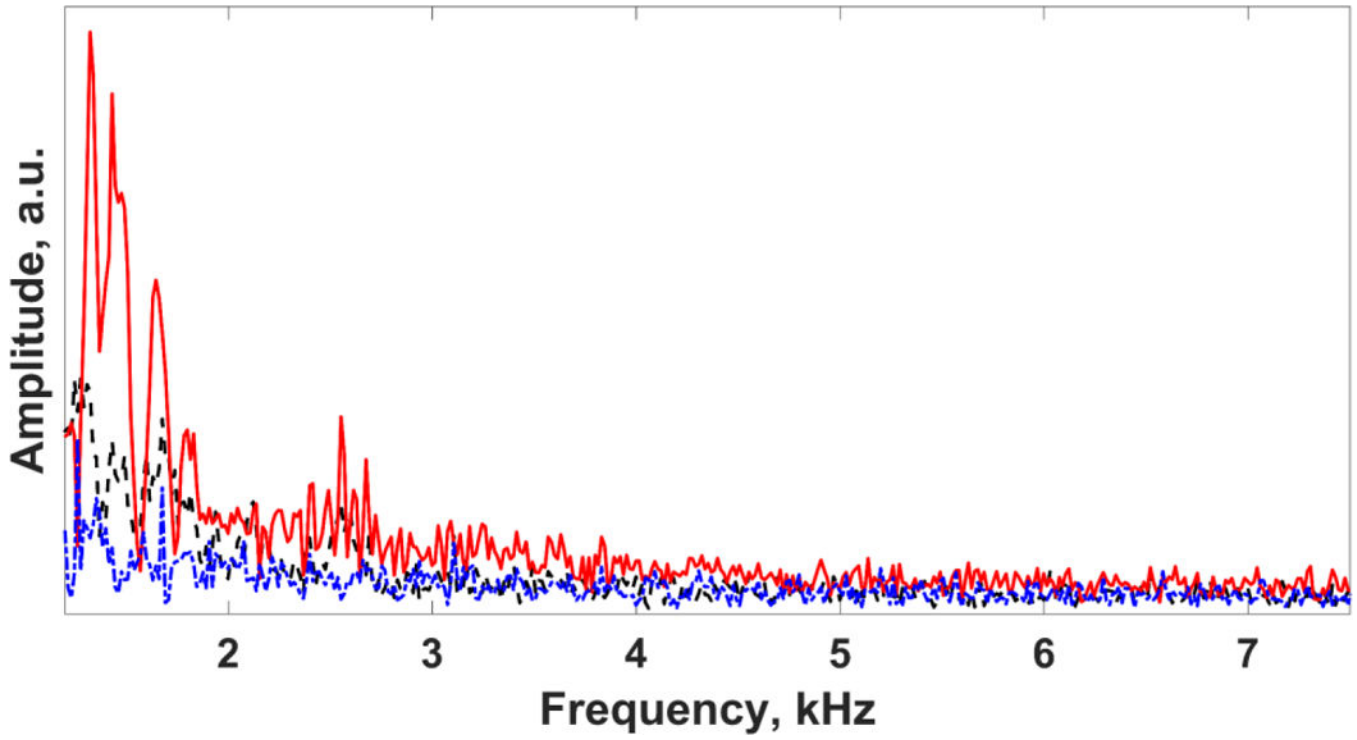

Figure 4.

Frequency dependence of the amplitude of the mechanical background signal measured with a 70 ms chirp of scan frequencies from about 1.2 to 7.5 kHz. The current in the rapid scan coils corresponds to a 13.7 G sweep width. Each trace was signal averaged for a total of 2.2 min data acquisition time. The incident power on the driven resonator was 65 mW. The background amplitudes were measured for B_0 = 0 G and zero gradient (blue dotted trace), B_0 = 91 G and zero gradient (black trace), and B_0 = 91 G and 10 G/cm z gradient (red trace).

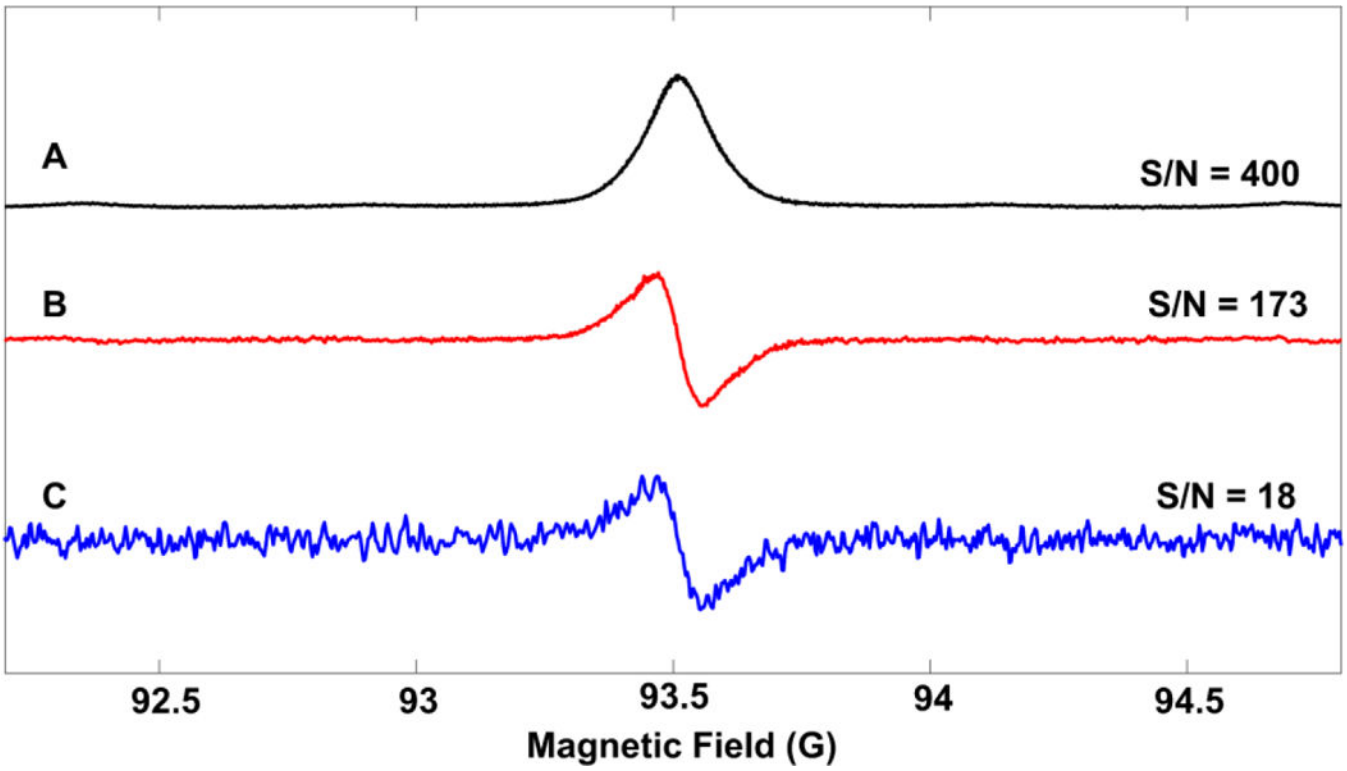

Figure 5.

Rapid scan and CW spectra of 0.1 mM OX63. (A) Sinusoidal rapid scan spectra. (B) Pseudo-modulated (24 mG) rapid scan spectra. (C) CW spectra. The effective filter for the rapid scan spectrum was the 2.5 MHz resonator bandwidth. The detection bandwidth was 5 MHz. The CW spectra were acquired using a Bruker Elexsys signal processing unit (SPU) with 5.2 ms conversion time, and 3-point binomial digital filter (n = 1 selected in the software; the number of points smoothed is 2n+1), which results in a filter time constant approximately equal to the conversion time, roughly 200 Hz. Hence, the CW bandwidth is about 1 percent that of the rapid scan.

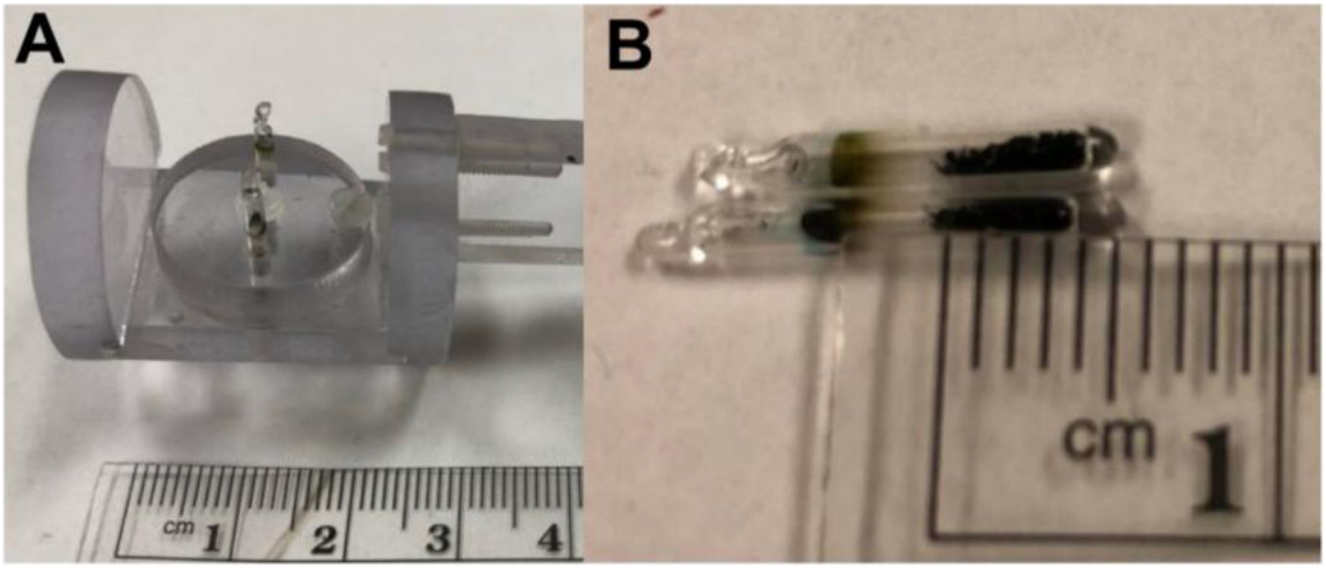

Figure 6.
(A) LiPc phantom consisting of two small LiPc samples separated by 1.0 cm. (B) Two LiPc samples, showing dimensions.

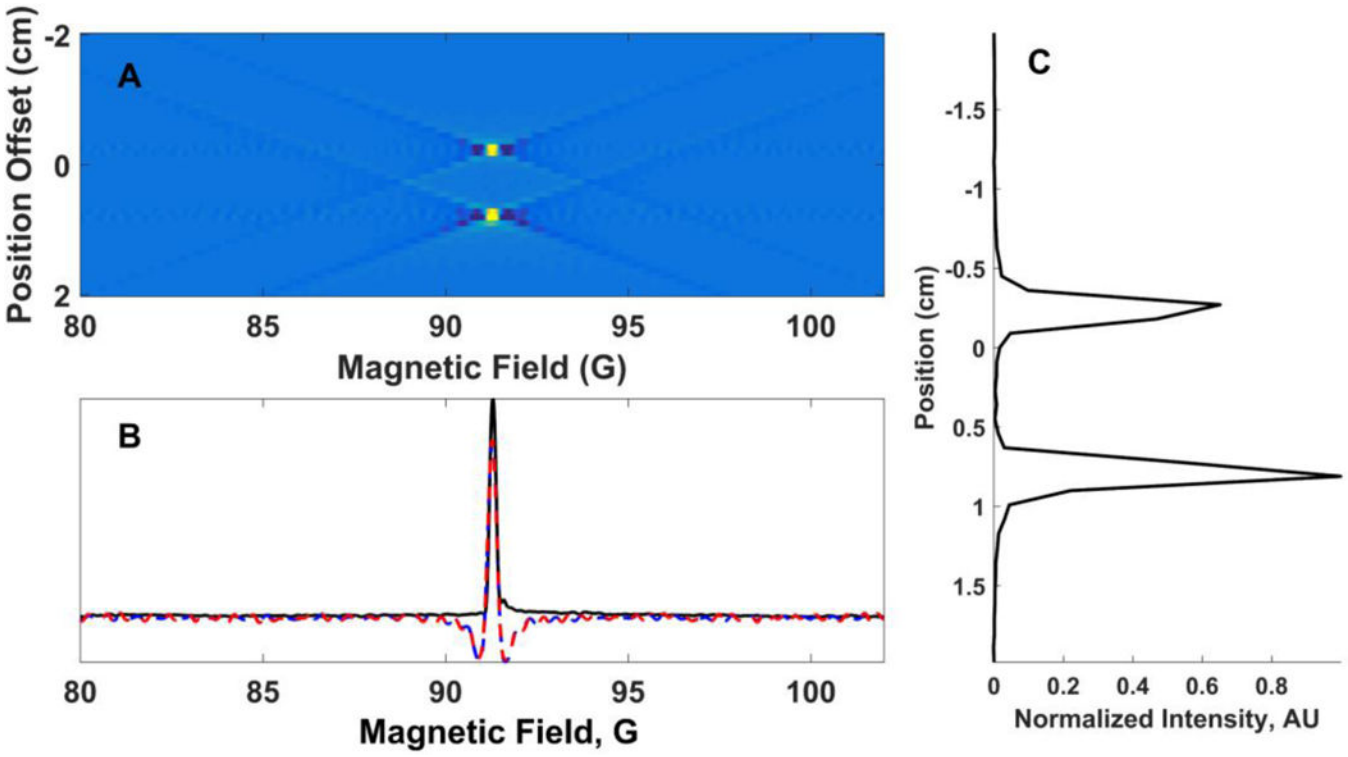

Figure 7.

(A) 2-D spectral-spatial image along Z of two LiPc samples (Figure 6A) separated by 1 cm. (B) Spectral slices (red and blue dashed lines) through the centers of the two samples (z = −0.27 and +0.81 cm) superimposed on the nongradient spectrum (black solid line). (C) Spatial slice through the centers of the two samples, B_0 = 91.4 G.

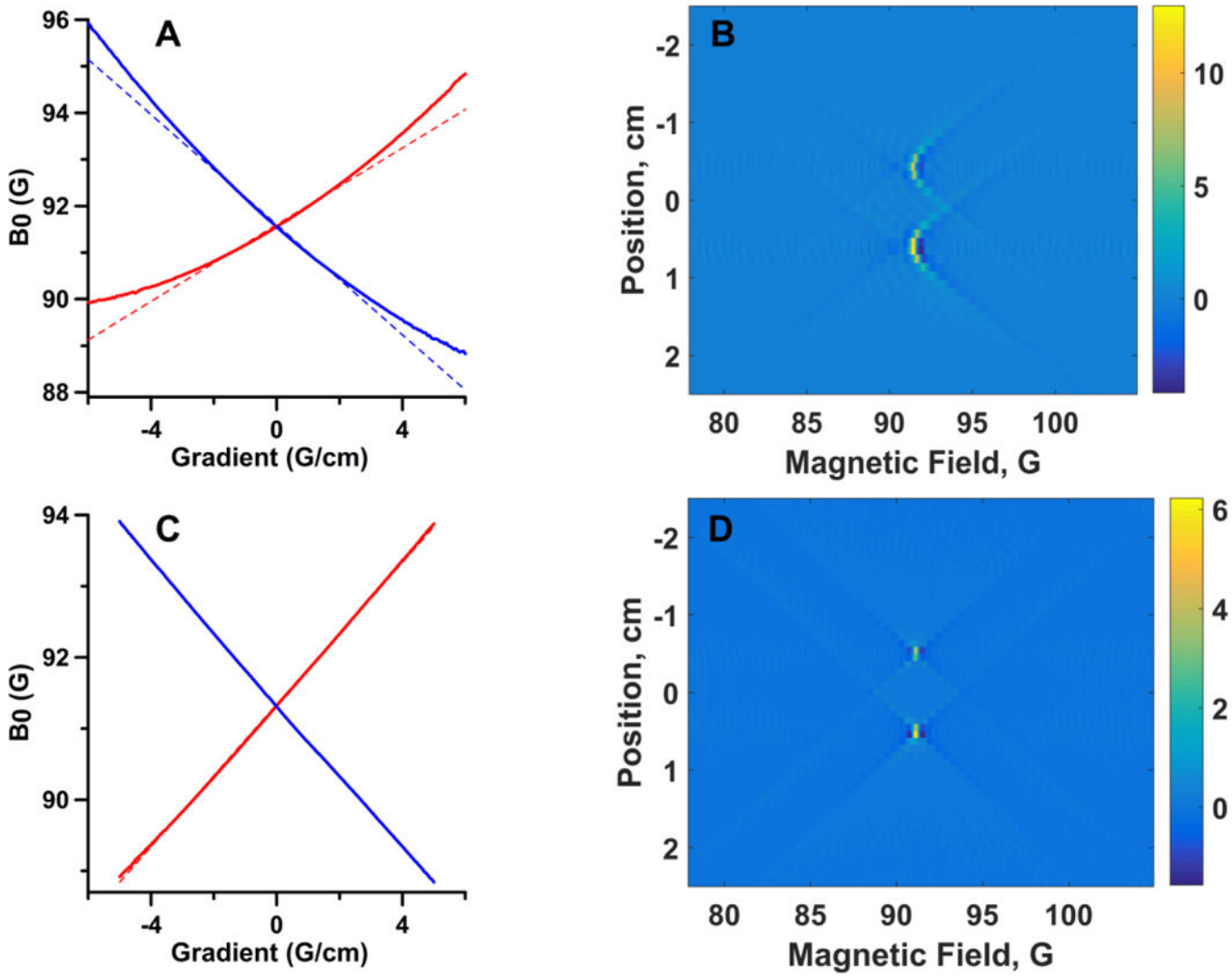

Figure 8.

(A) Plot of observed positions of signals for the two LiPc samples (red and blue solid lines) as a function of gradient. The predicted linear dependence of signal position on gradient is shown with red and blue dashed lines. (B) 2-D spectral-spatial image reconstructed from projections that included the off-axis contributions to the gradients to B_0 as shown in (A). (C) Positions of signals for the two LiPc samples (red and blue solid lines) at the same vertical location in the resonator as for (A), but at each gradient the value of B_0 was offset by an amount that is quadratic in gradient to correct for the effects of the concomitant gradients. The experimental data are superimposed on the predicted linear dependence of signal position on gradient (red and blue dashed lines). (D) 2-D spectral-spatial image reconstructed from projections acquired with the corrected center fields, as shown in (C).

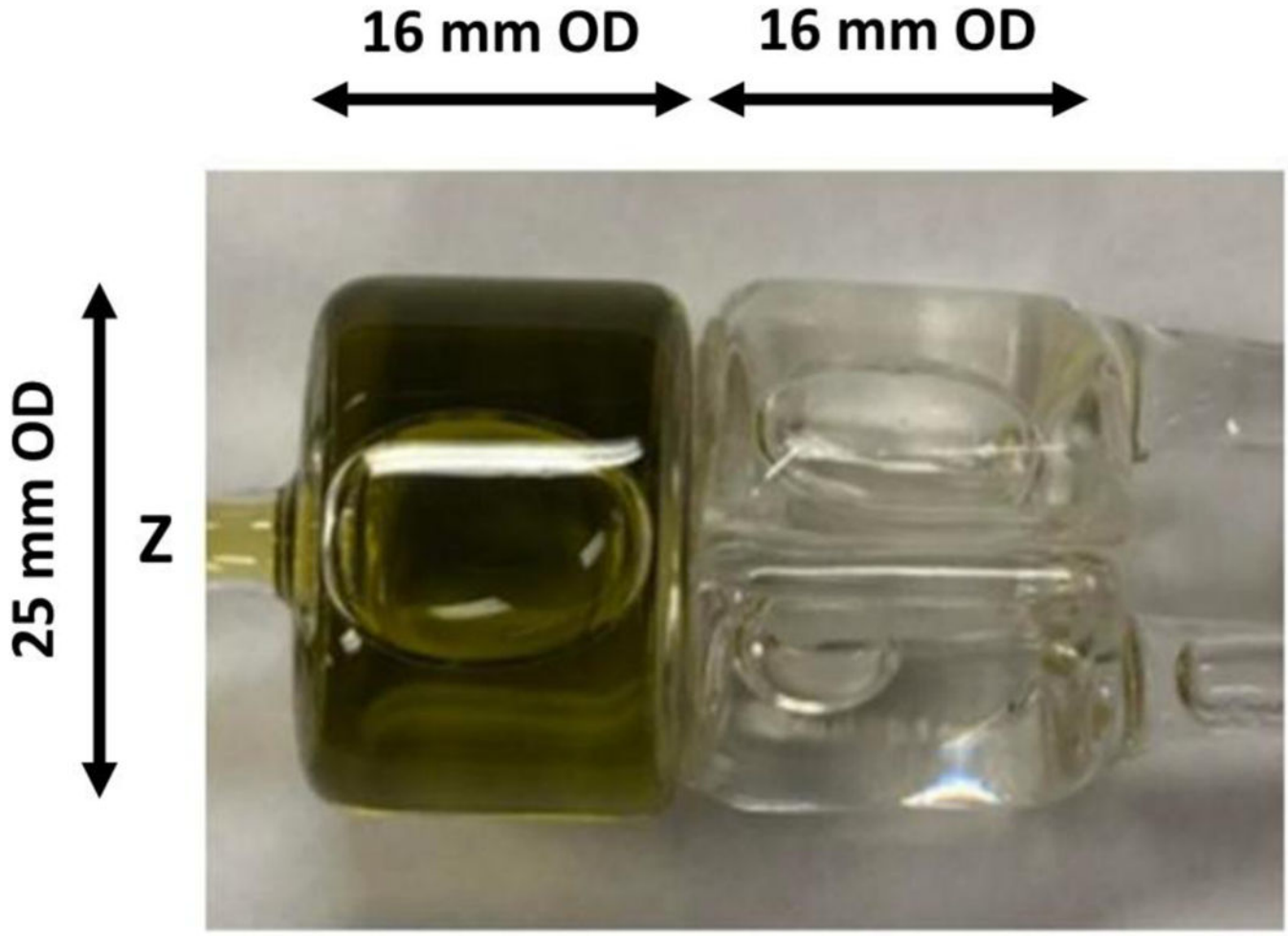

Figure 9.

Aqueous imaging phantom. The wall thickness of each tube is about 1.5 mm. On the left is 0.1 mM OX63. On the right is 1 mM ^{14}N Tempol (top) and 1 mM ^{15} N PDT (bottom) separated along the z-axis.

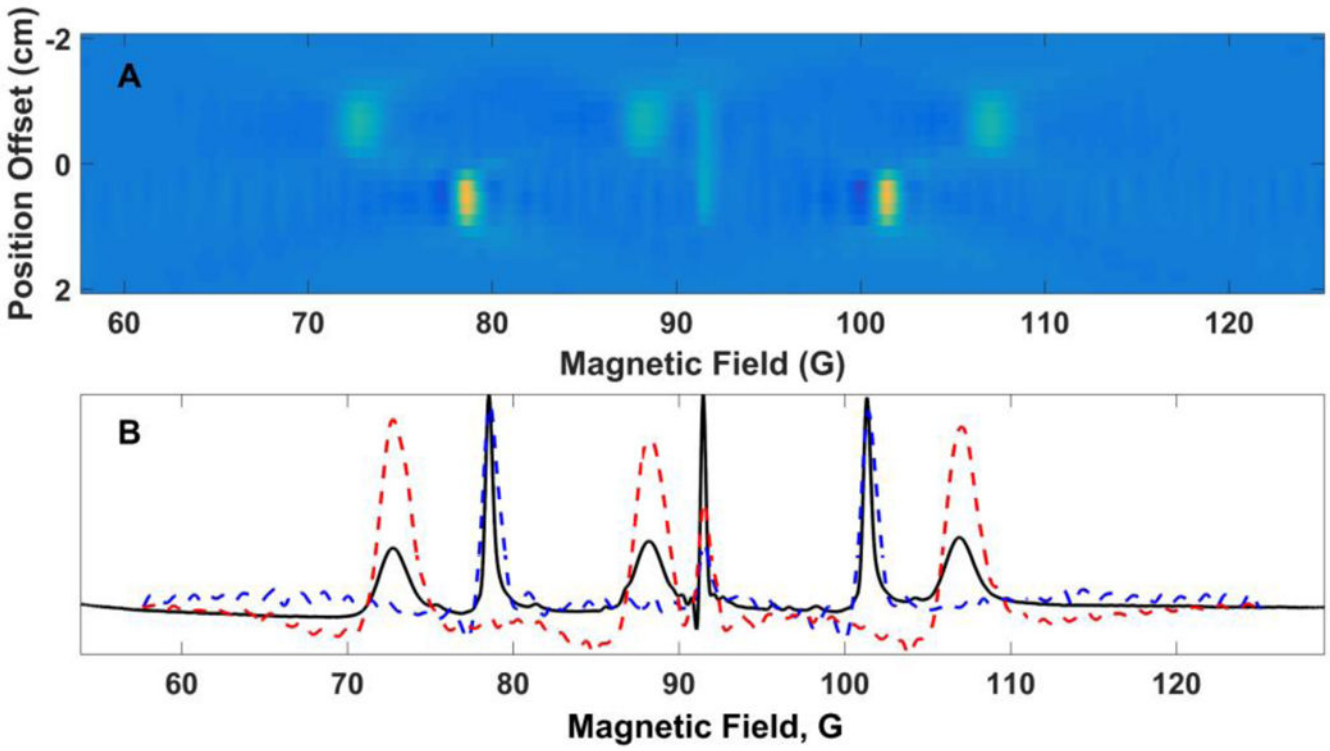

Figure 10.

(A) 2-D spectral spatial image along Z of aqueous phantom containing 0.1 mM OX63, 1 mM **14**N Tempol, and 1 mM ^{15}N PDT. The phantom shown in Figure 9. (B) spectral slices through the compartments containing OX63 and ^{14}N tempol (z = −0.72 cm, red dashed line) and the compartments containing OX63 and ^{15}N PDT (z = +0.64 cm, blue dashed line) are superimposed on the nongradient spectrum (black solid line).

Table 1

Resonator characteristics with and without sample.

	Empty	25 mm Aqueous Sample	Live mouse (whole body)[a]
Driven Resonator Coupling	−16 dB	−16 dB	−35 dB
Driven Resonator Frequency	254.6 MHz	254.2 MHz	253.75 MHz
Driven Resonator Q	50	50	40
Sample Resonator Coupling	−10 dB	−12 dB	−35 dB
Sample Resonator Frequency	237 – 263 MHz	233 – 257 MHz	253.75
Sample Resonator Q	78	78	23
Isolation Between Resonators	56 dB	60 dB	35 dB

[a]Mouse data provided by Subramanian V. Sundramoorthy, Center for EPR Imaging in Vivo Physiology, Department of Radiation and Cellular Oncoloy, University of Chicago, Illinois